Answer to anonymous Referee #1

Dear Referee #1,

We would like to thank you for the suggested revisions to our manuscript. The issues you raised were constructive and helpful to improve the quality of this paper and we have carefully considered them and revised this manuscript. Find enclosed our detailed answers to the comments that you raised.

Please note that the numbering of the Figures have changed since we added two new Figures. In our answers we refer to the updated Figure numbers and give the Figure numbers for the earlier version in brackets. Textual changes where we have considered your comments in the manuscript are given by page and line number for the updated document (uploaded as a supplement) and in brackets for the initial manuscript. Additionally, we have made a few changes where we felt the text could be improved and clarified.

Best regards,

Tobias Ahsbahs et. al.

Points for revision:
Major issues:

(1) The main point of this manuscript is the comparison between SCADA and SAR data and the ability of the SAR data to trace the wake of the wind farm. The manuscript should concentrate on this. Therefore, I suggest to skip the comparison with the WRF data. The WRF data are mentioned only marginally in the Abstract and in the Conclusions of the manuscript. This illustrates their minor importance for this investigation.

Answer: We find the results from WRF in Figure 6 (4) relevant to interpret the results obtained from SAR. We agree with you, that the results are not particularly present in the Abstract or the Conclusion but would like to highlight their importance there instead of omitting the result.
We find WRF modelling results are important here for two reasons: 1) 72 SAR images are the basis for calculations of non-dimensional mean wind speeds for row A. WRF results for the full time series and the coinciding time stamps show very similar results. We find it important to show the effect of downsampling in the model domain to support the selection of SAR images. 2) Both SAR and WRF (or other NWP models) are available before construction of a wind farm. In this case they agree well and we would argue that an agreement of two different data sets adds confidence to their accuracy. We would like to suggest to explore more cases in a future study to determine conditions where disagreement is found in wind speed variability over coastal waters.

Changes:
P22 L5 to L10 (P19,L25 to L26)
P22 L17 to L24 (P20,L2)
P24 L25 to L28 (P21,L19)

(2) There is considerable difference in data quality between SCADA and SAR data. First of all, SAR wind data at 10 m height is not a measurement but a product which arises from the stipulation of severe assumptions involving GMFs. That this could be a source of uncertainty is not even mentioned in the manuscript. Then, the 10 m SAR data must be extrapolated to the hub height of 81.6 m. This is done here by assuming a logarithmic wind profile. But the authors do not know how well this logarithmic profile depicts the reality. We know from earlier studies that the wind regime in the Baltic (Smedman and colleagues in the 1990s) is very often characterised by warmer air

over colder waters. This leads to the formation of internal boundary layers, low-level jets and non-logarithmic vertical wind profiles. This problem must be addressed in a manuscripts which intends to promote the use of SAR data in offshore wind energy especially in the Baltic.

Answer: Regarding general assumptions of the GMF to retrieve wind speed: This is a good point. We modified the manuscript in Sect. 2.2 to reflect more on the assumptions and uncertainties of SAR wind fields.

Changes:
P5 L1 to L9 (P4,L14)

Regarding stability correction, we added simulation results from WRF for the wind farm site to give indication about the atmospheric stratification (see Fig. 1) and moved the introduction of wind speed extrapolation into a separate subsection under Sect. 2.5. Using modelled stability results for extrapolation of SAR wind fields does not increase the accuracy compared with in situ measurement (Badger, M. et al., 2016. Extrapolating Satellite Winds to Turbine Operating Heights. *Journal of Applied Meteorology and Climatology*, 55(4), pp.975–991.). A simple stability correction assuming averaged profile to be near stable and near unstable has been implemented. These results shall illustrate the impact of stability of the upstream comparisons in Fig.4 (2) where the bias changes but the RMSE changes marginally. We have added a similar test for results presented in Fig. 6 (4) where the results are almost unaffected due to the presentation as a wind speed ratio. Additionally, we have raised this issue in the Discussion.

Changes:
Add Sect. 2.5 P6 L24 to P7 L10
P9 L13 to L17 (P7 L8 to L13)
P10 L8 to L9 (P8,L10)
P13 L16 to L22 (P11 L 16)
P22 L12 to L15 (omitted P19,L6 to L12)

Further issues:
(3) The first paragraph of the Introduction summarises the impact of inhomogeneous coastal areas on offshore wind fields. Here the work of Dörenkämper et al. should be mentioned (Dörenkämper, M., Optis, M., Monahan, A., & Steinfeld, G. (2015). On the offshore advection of boundary-layer structures and the influence on offshore wind conditions. Boundary-Layer Meteorology, 155(3), 459-482).

Answer: This is an interesting and very relevant study and we have added it to the Introduction.
Changes: P1,L27 (P1,L27):

(4) page 2, lines 22-27: aircraft measurements at hub height in the far wake of large offshore wind farms are now available. See: Platis, A., S.K. Siedersleben, J. Bange, A. Lampert, K. Bärfuss, R. Hankers, B. Cañadillas, R. Foreman, J. Schulz-Stellenfleth, B. Djath, T. Neumann, S. Emeis, 2018: First in situ evidence of wakes in the far field behind offshore wind farms. Scientific Reports, 8, 2163. DOI: 10.1038/s41598-018-20389-y

Answer: Thank you for pointing out this study. The results are extremely interesting. We added the reference to P2 L28 to L29 (P2 L26).

(5) page 2, line 2: a reference is missing

Answer: A link to copernicus.eu has been added on P3 L4 (P3,L2)

(6) page 2, line 8: wind farm parameterisation in WRF: here, the parameterisation available in WRF by Fitch should be mentioned: Fitch, A. C., Olson, J. B., Lundquist, J. K., Dudhia, J., Gupta, A. K., Michalakes, J., & Barstad, I. (2012). Local and mesoscale impacts of wind farms as parameterized in a mesoscale NWP model. Monthly Weather Review, 140(9), 3017-3038.

Answer: The reference has been added on P3 L11 (P3,L8)

(7) How has the correlation coefficient displayed in Figure 2 been computed? From the bin means (black diamonds in the Figure) or from the full data set (grey circles in the Figure)? It actually does not look like that the grey circles can be explained by such a high correlation coefficient.

Answer: The correlation has been calculated from the blue (gray if printed black and white) circles using the statistical tools implemented in the Software Mathematica 10.3. We did our own implementation of the correlation coefficient that confirms your suspicion of too high correlation coefficients. The problem seems to be a bug in the Mathematica software when forcing the fitting through the origin.

Figure 4 (2) and 5 (3) have been updated with the correct implementation of the correlation coefficient are now 0.74 and 0.78.

(8) What is displayed in the last line of Table 3?

Answer: The same as in line 2 but normalized with the wind speed at the center turbine of row A (turbine A15).

Changes: Caption of Table 3 P13 L7 to L8 (P11 L10)
U_{15} has been changed to U_{A15} to reflect more precisely that the wind speed at turbine location A15 is meant.

(9) Subchapter 3.3.2: it does not really become clear why there are no discernible wake effects in the "short fetch" case.

Answer: In order to determine wakes from SAR images before and after construction we need to assume that the wind conditions are similar between the two periods. This assumption is added more clearly to the manuscript. It is hard to draw a clear conclusions why the wake is not visible here. We made this uncertainty in the interpretation more clear.

Changes:
P13 L24 to L27 (P11,L19)
Removed (P15 L12)
P23 L14 to L18 (P20 L13)

(10) Chapter 3.4 and Figure 11 (related to the preceding comment): Figs. 11 c and d are in contradiction to Figs. 8 b and 9. While there are clear wake effects in Figs. 11 c and d, there are none in Figs. 8 b and 9. The wind direction in both groups of figure is nearly identical. This contradiction should at least be addressed in the manuscript. This contradiction seems to be a clear hint that SAR data is not easily interpretable (see the above comment no. 2).

Answer: We agree that there should be a better connection between these parts of the study. Additionally, we have added a more detailed explanation why transect b might be stronger affected by the differences in the

wind direction compared to transects c and d in P20 L7 to P21 L2. We agree that interpretation of SAR based wake is challenging, especially for fetch limited cases. We explicitly added the contradiction between Fig. 11 (9) and 13 (11) to motivate further studies.

Changes:
P20 L7 to P21 L10 (P17,L15 to P18,L2)
P23 L23 to L26 (P20,L18 to L21)

Applications of satellite winds for the offshore wind farm site Anholt

Tobias Ahsbahs[1], Merete Badger[1], Patrick Volker[1], Kurt S. Hansen[1], Charlotte B. Hasager[1]

[1]Department of Wind Energy, Technical University of Denmark, Roskilde, 4000, Denmark

Correspondence to: Tobias Ahsbahs (ttah@dtu.com)

Abstract. Rapid growth in the offshore wind energy sector means more offshore wind farms are placed closer to each other and in the lee of large land masses. Synthetic Aperture Radar (SAR) offers maps of the wind speed offshore with high resolution over large areas. These can be used to detect horizontal wind speed gradients close to shore and wind farm wake effects. SAR observations have become much more available with the free and open access to data from European satellite missions through Copernicus. Examples of applications and tools for using large archives of SAR wind maps to aid offshore site assessment are few. The Anholt wind farm operated by the utility company Ørsted is located in coastal waters and experiences strong spatial variations in the mean wind speed. Wind speeds derived from the Supervisory Control And Data Acquisition (SCADA) system are available at the turbine locations for comparison with winds retrieved from SAR. The correlation is good, both for free stream and waked conditions. Spatial wind speed variations along the rows of wind turbines derived from SAR wind maps prior to the wind farm construction agree well with information gathered by the SCADA system and a numerical weather prediction model. Wind farm wakes are detected by comparisons between images before and after the wind farm construction. SAR wind maps clearly show wakes for long and constant fetches but the wake effect is less pronounced for short and varying fetches. Our results suggest that SAR wind maps can support offshore wind energy site assessment by introducing observations in the early phases of wind farm projects.

1 Introduction

Europe now has a total installed offshore wind capacity of 15,780 MW (status as end of 2017) corresponding to 4,149 grid-connected wind turbines across 11 countries. By 2020, offshore wind is projected to grow to a total installed capacity of 25 GW (Wind Europe 2018). In Northern Europe much of this development is happening in the North Sea and the Baltic Sea. With an increasing amount of wind farms already erected, suitable locations with prevailing wind directions undisturbed by land or other wind farms are becoming scarce. Therefore, new wind farms are built in less favourable locations e.g. in the lee of land masses or large wind farms. Additionally, many shore lines are not straight but have a complex geometry that is determined by peninsulas, bays and islands. The lee effect of land i.e. the horizontal wind speed gradient due to a varying distance to shore (fetch) and wind farm wakes from other wind farms both influences the wind resource. Dörenkämper et al. (2015) found that large "horizontal streaks of reduced wind speeds that under stable stratification are advected several tens of kilometres over the sea" can severely affect offshore wind farms. Correct prediction of the wind resource influenced by

either land or adjacent wind farms, or a combination of the two, is a challenging problem. This study is motivated by this challenge and focuses on the Anholt offshore wind farm in the Kattegat Strait in Denmark. It involves analysis of satellite-based Synthetic Aperture Radar (SAR) wind maps, wind turbine data, and simulation results from the Weather Research and Forecasting (WRF) model.

Winds over the ocean can be remotely sensed by satellites carrying SAR systems (Dagestad et al. 2013). SAR systems transmit and receive microwaves and the radar backscatter signal is very sensitive to small-scale ocean waves. This scattering mechanism is diffuse and known as Bragg scattering (Valenzuela 1978). The wind causes cm-scale waves to form on the ocean surface that are in local equilibrium with the wind speed. The wind speed at 10m height can be retrieved from SAR observations via an empirical Geophysical Model Function (GMF) (Stoffelen & Anderson 1997; Quilfen et al. 1998; Hersbach 2010). The major advantages of SAR imagery, in terms of applications for wind energy, lie in the high spatial resolution and the coverage of large areas with swath widths of several hundred kilometres.

Coastal wind speed gradients have previously been quantified from SAR wind maps and compared to model simulations by Barthelmie et al. (2007) based on the very limited number of satellite samples available at the time. Ahsbahs et al. (2017) showed that sea surface wind speeds retrieved from SAR compare well with scanning lidar wind observations as close as 1 km from the coastline. Mapping of the mean wind speed from SAR consistently shows a wind speed gradient with increasing distance from the coastline for the seas around Northern Europe (Hasager et al. 2011; Hasager, Mouche, et al. 2015). At the Anholt wind farm, Peña et al. (2017) have shown strong variability of the wind speed within the turbine rows for wind directions where the land is upstream. A correct prediction of this coastal gradient is desirable for optimal placement and layout of wind farms.

Many studies of wake effects around large offshore wind farms are focused on wake interaction within the wind farms or between closely adjacent wind farms (Barthelmie et al. 2010; Hansen et al. 2012; Nygaard 2014; Hansen et al. 2015; Volker et al. 2015; Nygaard & Hansen 2016). Investigations of wind farm wake effects based on SAR wind maps have revealed the existence of extensive wakes under certain atmospheric conditions (Christiansen & Hasager 2005; Christiansen et al. 2006; Li & Lehner 2013; Hasager, Vincent, et al. 2015). The SAR wind maps contribute with information about the far-wake field, which is typically not available from other sources. Recently, the first airborne in-situ measurements of the far-wake became available showing that wind farm wakes frequently extend over several tens of kilometres (Platis et al. 2018).

A systematic use of SAR wind maps by the offshore wind energy industry has been lacking due to three limitations: i) SAR observations are made at the sea surface, while wind turbine rotors operate between 30 m and 250 m height; ii) SAR images have a low temporal sampling rate on the order of a few hundred images per year, depending on the location on Earth; and iii) SAR wind retrieval has required expert skills and substantial processing capabilities. These issues have been partially

overcome: A method for extrapolation of mean wind speeds retrieved from SAR at 10 m above sea level to the wind turbine hub height has been developed (Badger et al. 2016) and a number of new SAR sensors have been launched in recent years, which increases the sampling rate and ensures continuity. The access to SAR observations and derived products, such as wind maps, is eased significantly through the Copernicus programme[1] and its downstream services.

Numerical Weather Prediction (NWP) models perform simulations of wind speed and wind direction as well as other atmospheric variables for long time series with frequent data (e.g. hourly) at several heights in the atmosphere. The WRF model (Skamarock et al. 2008) has been used to assess offshore wind resources. Good results are obtained in the open sea but in coastal regions near upstream land mass the uncertainty increases (Hahmann et al. 2015). Wind farm wakes are not simulated by NWP models unless the effect of wind turbines to the atmospheric flow are parametrised (Volker et al. 2015; Fitch et al. 2012). Engineering wind farm models like the Park model (Jensen 1983), Fuga (Ott et al. 2011), and the G. C. Larsen model (Larsen 2009) have been used in combination with WRF outputs (Peña et al. 2017).

Supervisory Control And Data Acquisition (SCADA) data is available from the wind turbines at Anholt and 10-minute mean wind speeds can be inferred from those measurements (hereafter SCADA wind speed). This data set gives a unique opportunity to characterize the spatial variability of the wind speed within the wind farm and it is a baseline for comparisons with wind speeds from SAR and WRF in our analyses.

The objective of this study is to demonstrate the prediction capability of SAR imagery for an offshore wind farm site where coastal wind speed gradients and wind farm wakes interact in a complex fashion. To establish confidence in the SAR wind retrievals, we first compare wind speeds from SAR and SCADA in free stream and in wake conditions. To determine whether archived SAR wind fields can predict the spatial wind speed variability at Anholt, we analyse the mean wind speed along the most Western turbine row before and after the wind farm construction. The wind farm wake effect is quantified through comparison of mean wind speeds from SAR upstream and downstream of the wind farm. Finally, the interplay between coastal wind speed gradients and wind farm wake effects is investigated through analysis of SAR wind speeds along transects perpendicular to the coastline.

The paper is structured as follows: Section 2 introduces the location, the data sets, and pre-processing used. Section 3 addresses the methods and results. In Sect. 4, we discuss implications of the presented results for wind energy projects and in Sect. 5, we conclude on the use of SAR for characterizing coastal wind effects and wind farm wakes.

[1] http://www.copernicus.eu/

2 Location & Data

This section describes the wind farm site Anholt and the data sets and pre-processing steps used for our analyses.

2.1 Anholt wind farm

The Anholt Offshore Wind Farm is located in the Kattegat Strait of Denmark in the waters between Djursland and the island of Anholt in an area with fairly consistent water depths of about 15 to 19 metres, see Figure 1. The Anholt Offshore Wind Farm is approximately 20 km long and up to 8 km wide. The shortest distance to Djursland is 16 km, while there are 21 km to the island of Anholt. The Anholt wind farm consists of 111 Siemens SWT-120- 3.6 MW wind turbines with a rotor diameter of 120 m with a total capacity of 400 MW and it was constructed during 2012-2013. The internal wind turbine spacing is 5-7 rotor diameters.

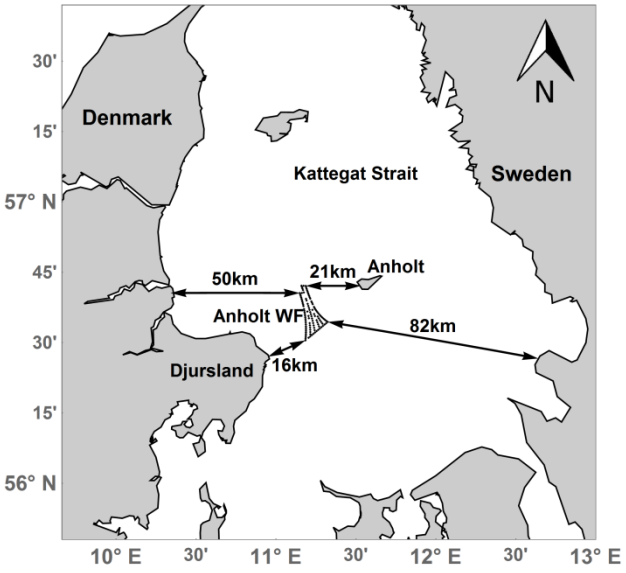

Figure 1: Position of the Anholt wind farm (Anholt WF) and distances to the coast.

2.2 SAR wind fields

Wind fields retrieved from two different satellite SAR missions are used in this study. Envisat ASAR from the European Space Agency (ESA) acquired images between August 2002 and April 2012 before the construction of the Anholt wind farm. The mission was followed up by a constellation of two ESA satellites, Sentinel-1A and B, from which data is available since December 2014 and April 2016, respectively. Data until May 2017 is included for this study. The entire Sentinel-1 data series is recorded after construction of the wind farm at Anholt. The Copernicus programme publishes Envisat and Sentinel-1 A/B images under an open access license, allowing for unlimited use, both for research and commercial applications.

SAR wind retrievals are indirect estimates of the wind speed that rely on the assumption that a measurement of the radar backscatter from the sea surface can be converted to a corresponding wind speed at the height 10 m. This is possible because the SAR observations are sensitive to cm-scale waves at the sea surface, which are generated by the instantaneous wind stress. Phenomena that modify the small-scale ocean surface waves i.e. biological or mineral films (Gade & Alpers 1997), and sea states (Alpers et al. 1981) influence the wind speed retrieval. This adds uncertainties to the wind speed retrieval. Global validation studies of satellite wind retrievals against modelled wind speeds found RMSE of 1.30 m/s (Hersbach 2010) while validations against in situ measurements in the Baltic showed an RMSE of 1.17 m/s (Hasager et al. 2011). Both studies show that while the accuracy of individual wind speed retrievals is somewhat low, SAR wind fields capture the mean wind speed and its spatial variability well.

An archive of processed wind maps from Envisat and Sentinel-1 A and B over Europe is available from DTU Wind Energy[2]. Our analyses are based on these readily available SAR wind maps. In the archive, wind speeds are retrieved from the SAR scenes using the SAR Ocean Products System (SAROPS) (Monaldo et al. 2015). The GMF called CMOD5.N (Hersbach 2010) is chosen for the wind speed retrieval, and wind directions are needed as an ancillary input for processing. We obtain the wind directions from the Climate Forecast System Reanalysis data set (CFSR[3]) during 2002-10 and from the Global Forecasting System (GFS[4]) during 2011-17. To reduce effects of random noise in the SAR imagery and to smooth out effects of longer period waves that modify the local radar incidence angle, the SAR scenes are resampled to 500-m pixel size in connection with the wind retrieval processing. Hard targets like wind turbines or offshore substations cause a strong signal in SAR images. The increased backscatter signal will cause an overestimation of the retrieved wind speed and therefore, extremely bright resolution cells are filtered out of the SAR wind maps prior to our analyses.

2.3 SCADA data

SCADA systems monitor record wind turbine data, i.e. power production or pitch angle. The wind turbine power curve links the free wind speed to a power production. This wind speed (hereafter SCADA wind speed) can be derived from power and pitch combined with the power curve provided by the turbine manufacturer. The power is monotonically increasing with the wind speed between cut-in and rated power. Therefore, the wind speed can be inferred for this region. From rated power to cut-out, the power is constant but the blades are pitched increasingly. For this region, the wind speed can be inferred from the pitch signal. The resulting wind speed is equivalent to the reference wind speed used to create the power curve and is treated as a measurement at hub height. An inter-comparison between the turbines reveals that this is - in general an acceptable approach.

[2] https://satwinds.windenergy.dtu.dk
[3] http://nomads.ncdc.noaa.gov/data.php?name=access#cfs-reanal-data
[4] http://nomads.ncdc.noaa.gov/data/gfsanl

A qualification procedure is used to eliminate periods where the wind turbines are not grid connected and are not producing power during a complete 10-minute period or have been curtailed, meaning their power generation has been reduced. Unfortunately, the wind speed for turbine A05 deviates due to unknown reasons and will be excluded from the analysis. The remaining periods are applicable for analysis after a final examination of the power curve. Due to a lack of undisturbed mast measurements, the inflow conditions need to be derived from the operational wind turbine data themselves. The inflow reference wind direction is determined from calibrated, undisturbed selected wind turbine yaw positions on the edge of the wind farm (cf. Peña et al. (2017) for further details).

2.4 Numerical wind simulations

The numerical simulations used in this study are performed with WRF version 3.5 without wind farm parametrization. The total simulated period covers 28 years from 1990 to 2017. Simulations are performed in 10-day chunks. Each individual simulation extends in total over 11 days, with the first day being disregarded as a spin-up period. The computational domain consists of three nests with an 18 km, 6 km, and 2 km grid spacing, respectively. Here the outermost domain is forced by (ECMWF) ERA-Interim Reanalysis (Dee et al. 2011) and the results of the inner-most domain are used for the analysis. In the horizontal direction, the innermost domain extends over 854 km and 604 km in the x and y direction. In the vertical direction, 41 vertical levels with model top at 50hPa are used, with 9 levels being within 1000 m from the surface. Wind speeds at the turbine hub height are derived by logarithmic interpolation between the two closest model levels.

The most relevant physics parametrizations in the model set-up, are the Yonsei University Scheme (YSU) Planetary Boundary Layer (PBL) scheme (Hong et al. 2006) and the MM5 similarity surface-layer scheme, and Sea surface temperatures from NOAA/NCEP (Reynolds et al. 2010). Further details of the model set-up and its validation are given in Peña & Hahmann (2017). WRF wind directions at the same locations as for the SCADA derived wind direction are extracted and averaged to a time series of representative wind directions.

2.5 Wind speed extrapolation

SAR wind speeds are retrieved for a height of 10 m and SCADA wind speeds are representative for the wind turbine hub height at 81.6 m. A wind profile needs to be applied to perform wind speed extrapolation between these two levels. Ideally, the local stratification should be considered but no measurements that could lead to a quantification of atmospheric stability effects are available on site. In lack of local measurements, we assume a logarithmic wind profile with a wind speed dependent roughness length using Charnock's relation and the Charnock parameter (Grachev & Fairall 1996). Later we test this assumption through a sensitivity analysis using stability correction to the logarithmic wind profile (Wyngaard 2010, p 222).

The WRF model outputs include stability information expressed as the length scale z/L. We use this to investigate the frequency of occurrence for different stability classes. Stability information from WRF is not sufficiently accurate to perform a stability correction of the wind profile for individual SAR samples (Badger et al. 2016). Stability classes at the turbine hub height are defined using the definitions from Hansen et al. (2012) for WRF simulations coinciding with the SCADA time series at the wind farm location, see Figure 2. The WRF outputs indicate that neutral stratification is increasing with the wind speed and the overall distribution favours stable stratification over unstable at the Anholt site. These findings differ from simulation and measurements of stratification in the Baltic, which favour stable stratification (Smedman et al. 1997).

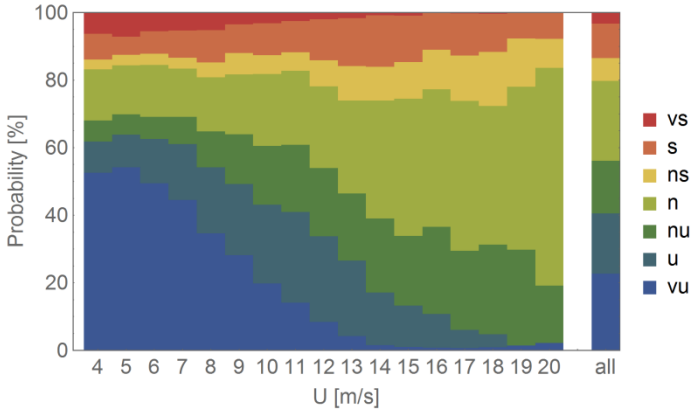

Figure 2: Distribution of 7 stability classes from very stable (vs) to very unstable (vu) based on 2.5 years of WRF simulations for wind speeds between 4 m/s and 20m/s (left) and the distribution for all wind speeds (right).

3 Methods & Results

Four different methods are applied to analyse SAR wind fields around the Anholt wind farm. These are listed in Table 1 together with the temporal coverage for SCADA, SAR, and WRF data used in the respective analysis. The SCADA winds are used as reference measurements. "Wind direction" specifies the data input used for selection of SAR wind fields in contrast to the wind direction used for the SAR wind retrieval described in Sect 2.2. Averaged wind speeds can show strong gradients in two directions. In the following, the term 'wind speed gradient' refers to wind speed changes perpendicular to the coastline whereas the term 'wind speed variability' refers changes along the rows of wind turbines. For SAR based wake studies in Sect 3.3 and 3.4 we assume that all turbines at Anholt are operational. Data about the overall turbine availability is not available for publication for proprietary reasons.

Table 1: Overview of the data sets and time periods used for the analysis.

Analysis	SCADA wind	SAR wind	WRF wind speed	Wind direction

3.1 Comparison of wind speeds from SAR and SCADA	12.2014 – 06.2015	12.2014 – 06.2015	–	SCADA
3.2 Wind speed variability along Row A	01.2013 – 06.2015	08.2002 – 04.2012	01.2002 – 12.2012	SCADA/WRF
3.3 Wind farm wakes from SAR	–	08.2002 – 04.2012 12.2014 – 05.2017	–	WRF
3.4 Wind farm wakes and gradients	01.2013 – 06.2015	08.2002 – 04.2012 12.2014 – 05.2017	–	WRF

3.1 Comparison of wind speeds from SAR and SCADA

Comparisons between SAR wind speeds and SCADA winds are carried out upstream (free stream conditions) and downstream (wake conditions) of the wind turbines at Anholt. SAR wind maps at a resolution of 500m need to be further averaged in order to better represent the wind conditions measured as 10-minute means at the turbine locations (Christiansen & Hasager 2005). SAR wind speeds at the turbine locations are contaminated by reflection from the wind turbines. It is thus necessary to extract resolution cells on the upstream or downstream side of the turbines, respectively. We extract and average SAR resolution cells within a hexagonal footprint inspired by the method of Gash (1986). The method was previously applied to SAR wind maps by Hasager et al. (2004). The hexagonal shape is aligned with the wind direction and extends from 600m to 2600m from each turbine with a maximum width of 1200m. Wind directions from SCADA are used for the directional alignment. Figure 2b shows example footprints for a situation with Westerly winds. Resolution cells are extracted from the SAR wind maps if their center point falls within the footprints defined. Within each footprint, the average wind speed is determined and compared with the corresponding SCADA wind speed. Comparisons are done along the turbine rows A, P and 1 on the edge of the wind farm for the wind direction intervals shown in Table 2.

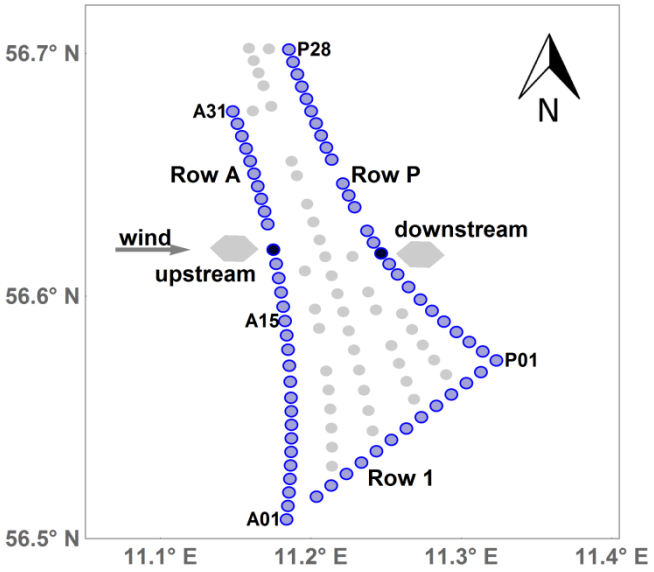

Figure 3: Sketch of the Anholt wind farm where turbines in rows A, P and 1 are used for comparisons and marked in blue. The remaining turbines are located at the grey circles. The grey hexagons are examples of footprints used for extracting the average SAR wind speeds upstream and downstream of the wind turbines for an example wind direction of 270°. The turbines used for comparisons in this example are marked in black.

Table 2: Wind direction ranges for SAR/SCADA comparisons for upstream and downstream comparisons.

	Row A	Row 1	Row P
upstream	210° to 330°	80° to 210°	10° to 100°
downstream	30° to 150°	260° to 30°	190° to 290°

Logarithmic wind profiles are used to extrapolate SAR wind speeds up to the turbine hub height at 81.6m. Extrapolation of SCADA winds from hub height down to 10 m, where the SAR winds are retrieved, is included as well since references on SAR wind speed accuracy are given for this height. The following results are based on SAR wind maps from 47 Sentinel-1A images collocated with the available SCADA data.

3.1.1 Upstream

Comparisons at hub height upstream of the wind turbines are shown in Figure 4. SCADA wind speeds at hub height range from 4 m/s to 20 m/s covering most of the range of wind turbine operation. Comparisons with SAR wind speeds yield a mean bias of -0.16 m/s, meaning a slight tendency of SAR to estimate higher winds. The correlations coefficient (R^2) of the linear fit through the origin is 0.74, the slope of the fit is close to one, and the RMSE is 2.33 m/s. Wind speeds at 10m in Figure 4b are generally lower and the RMSE of the comparison is lower due to this (1.80 m/s).

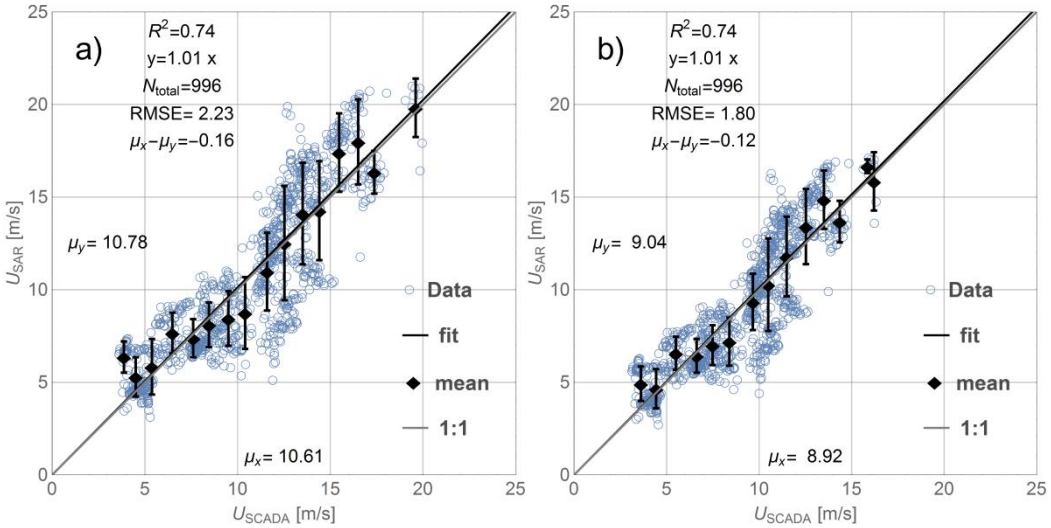

Figure 4: Comparison between SCADA derived wind speeds (U_{SCADA}) and SAR derived wind speed (U_{SAR}) upstream of the wind turbines: a) for the turbine hub height (81.6 m), b) for the reference height 10 m.

The low bias, good correlation and slopes close to one suggest that averaged SAR wind speeds are a good representation of the wind conditions as experienced by the wind turbines under free stream conditions. Using the wind direction from the SCADA system for the SAR wind retrieval process reduces the RMSE by approximately 0.1 m/s (not shown). This is a small improvement compared to the overall accuracy of the SAR wind retrieval, thus supporting the SAR processing choice. Assuming near stable and near unstable stratification changes the RMSE Figure 4b by less than 0.1 m/s but it does change the bias to -0.68 m/s and 0.19 m/s respectively.

3.1.2 Downstream

Figure 5 shows comparisons of SAR and SCADA wind speeds on the downstream side of the wind turbines for wind direction intervals defined in Table 2. At hub height, the averaged SCADA wind speed is 10.20 m/s and comparisons to SAR give a bias of -0.64 m/s, again towards higher wind speeds from SAR. The correlation coefficient of 0.78 is good for a linear fit with a slope of 1.06, and the RMSE is 2.12 m/s. Again, the correlation coefficient and the slope at 10m height are similar whereas the RMSE is lower (1.7 m/s). The mean bias is numerically smaller at 10 m (-0.50 m/s) than at hub height (-0.64 m/s).

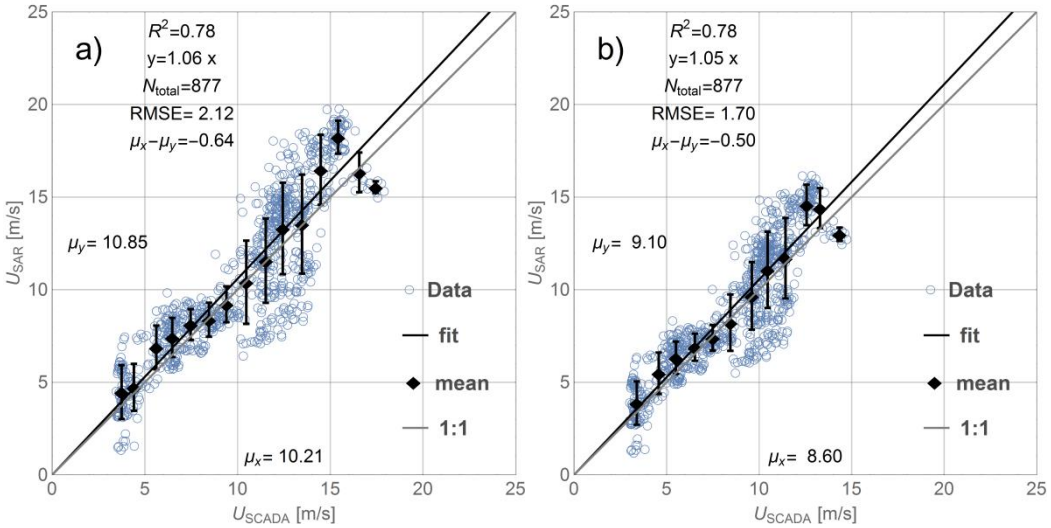

Figure 5: Comparison between SCADA derived wind speeds (U_{SCADA}) and SAR derived wind speed (U_{SAR}) downstream of the wind turbines: a) for the turbine hub height (81.6 m), b) for the reference height 10 m.

The bias is numerically higher downstream compared to upstream of the wind farm whereas the RMSE for downstream conditions is approx. 0.1 m/s lower than for upstream conditions. The lower RMSE seems counterintuitive, since we expect the assumption of a single logarithmic wind profile from the surface to hub height to be better satisfied upstream than downstream of the wind turbines due to wake effects. The number of observation pairs is higher upstream (996) than for downstream (877) as a result of the SAR image coverage and a reduced number of turbine locations downstream for the prevailing Westerly wind directions. The sampling difference may influence our results.

3.2 Wind speed variability along Row A

Observations of the past wind conditions are typically used in wind resource assessment to estimate the wind conditions a potential wind farm would be exposed to. Satellite SAR observations are available 10 years before the wind farm at Anholt was constructed. Peña et al. (2017) have shown a large variability of mean wind speeds for the Western row A between 245° and 275° from SCADA and WRF results. They are created by the roughness change between land and sea and are determined by differences in fetch caused by the shape for the peninsula (Van Der Laan et al. 2017). Here we investigate whether the variability of the mean wind speed at the site could be predicted from SAR wind maps prior to the wind farm construction. Our analysis of SAR wind maps is complemented by an analysis of numerical simulations from WRF, which are also available to a developer prior to the wind farm construction. The overall data availability for SCADA, SAR, and WRF is shown in Table 1 and the number of observations used in this analysis is shown in Table 3.

SAR wind speeds at the turbine locations of Row A are extracted as described in Sect. 3.1 for upstream situations. For the WRF simulations, hourly WRF wind speeds at hub height are interpolated for each of the turbine locations before they are

averaged. Both data sets are filtered according to the following conditions: i) Wind directions are between 245° and 275°, ii) there is full availability of measurements for all turbine locations along Row A; and iii) wind speeds averaged over row A are above the cut-in wind speed of the wind turbine. The averaged wind speeds are nondimensionalized through division with the respective wind speed at turbine position A15 (see Figure 3) giving a relative measure of wind speed variability along Row A.

The wind speed variability from SAR and WRF is first examined using two different sampling scenarios for the WRF simulations: the full WRF data set (2002 to 2012) and the WRF samples collocated with the SAR scenes, see Figure 6a. For both scenarios, the WRF simulations show a smooth and monotonically increasing mean wind speed from South to North along Row A. The maximum deviation of mean wind speeds from the two WRF data sets is below 0.5%. This suggests that the reduced sampling rate, which corresponds to the sampling of SAR observations, has little effect on the mean wind speed. The wind speed variability from SAR observations is less smooth and shows a local maximum at turbine A23. SAR winds are increasing from South to North until they stay approximately constant from turbine A24 on. The wind speed variability from SAR is in good agreement with the two WRF data sets from turbine A01 until A25 where the SAR wind speeds start to decrease.

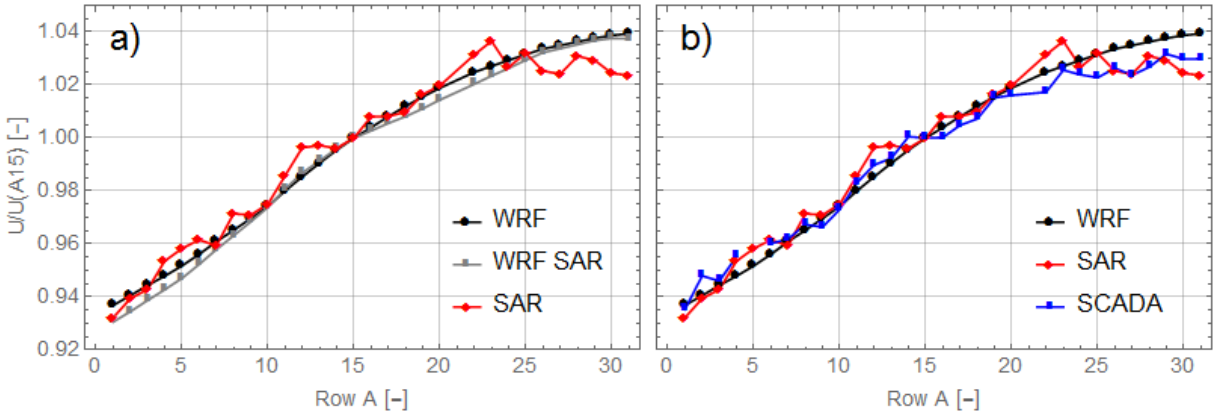

Figure 6: Average wind speed relative to turbine A15 for wind directions between 245° and 275°. a) Data from WRF (2002-2012) and SAR (2002-2012). The entire time period is used for "WRF" and WRF data coinciding with SAR images are used in "WRF SAR". b) Data from full WRF time series, SAR, and SCADA (2013-2015). No turbine was erected at location A21.

The relative mean wind speeds from SAR and WRF along Row A are compared to SCADA wind speeds in Figure 6b. All available data from both SAR and WRF before wind farm construction are used to best approximate the wind speed climatology from each data set. The SCADA winds, in contrast, cover a shorter period after the wind farm construction. There is a clear increase of the wind speed from turbine A01 until A20 in agreement with both the SAR and WRF data sets, but the result for turbine A05 has been left out as mentioned in Sect. 2.3. From position A24, SCADA and SAR winds show a similar behaviour whereas WRF winds are consistently higher and with less spatial variability. We can summarize the

findings above as wind speed differences between the Southern-most and Northern-most turbines. The difference $\Delta U_{N,S}$ is defined as:

$$\Delta U_{N,S} = \sum_{i=A28}^{A31} U_i - \sum_{i=A01}^{A03} U_i \quad (1)$$

Where U_i is the mean wind speed at the turbine location. The difference between the Northern and the Southern part of the wind farm is given in Table 3. SCADA and SAR agree within 0.1 percentage point while WRF predicts a 1 percentage point larger difference than SCADA results suggest.

Table 3: Sample sizes, difference between wind speed at the most Northern and Southern turbines $\Delta U_{N,S}$ (three turbine location averaged, see Equation 1), and the same difference normalized with the wind speed at turbine U_{A15} at turbine A15.

	SAR	WRF SAR	WRF	SCADA
Samples N [-]	72	72	10524	4625
$\Delta U_{N,S}$ [m/s]	0.92	1.02	0.98	0.95
$\Delta U_{N,S}/U_{A15}$[%]	8.8	10.3	9.8	8.7

The wind speed variability along Row A, as shown in Figure 6 and Table 3, is likely caused by varying fetch from the coastline of Djursland. The fetch at different positions along Row A can vary between 16 km and 50 km for the same wind direction, see Figure 1. The agreement between nondimensional wind speeds from SAR and SCADA is remarkably good. We can conclude that for this site, wind speeds retrieved from SAR imagery could have predicted the relative wind speed gradients well, before construction of the wind farm.

We test the influence of extrapolation by assuming the turbine hub height is within the surface layer and that both the atmospheric stability and the aerodynamic roughness length are constant along turbine row A. The relative wind speed should thus show little dependence of the height since the stability correction term has the same value. This has been tested assuming near stable and near unstable conditions. The resulting extrapolated wind speed (not shown) differs between -0.4 m/s (unstable) and 0.6 m/s (stable), while the results relative to turbine position 15 show differences below 0.01 percentage points. These assumptions will not be valid at all times, but the extrapolation error of the mean wind speed from 10m to hub height is expected to be reduced when the mean wind speed is divided by the mean wind speed at a reference location.

3.3 Wind farm wakes from SAR

To investigate the impact of the Anholt wind farm on the wind conditions in the area, we compare wind speeds extracted from SAR wind maps along two transects before and after wind farm construction. With this approach, a baseline of wind conditions before wind farm construction can be determined assuming that the wind conditions in the period before and after the wind farm construction are similar.

Wind farm wakes at Anholt are analysed for two wind direction sectors. The first sector (75°-105°) represents easterly wind directions and a long fetch. The second sector (255°-285°) represents Westerly wind directions and a short fetch, see Figure 1. Wind direction information from WRF is used for the selection of SAR wind maps within the two sectors as described in Sect. 2.4. Three additional criteria are set for SAR wind fields to be included in this analysis: i) the images must fully cover both transects; ii) the mean wind speed at 10m over the inflow transect is within the interval 3-12 m/s where we expect wind farm wakes to be strongest; and iii) visual inspection does not show any strong signals that are uncorrelated with the wind speed, e.g. rain contamination.

Figure 7 shows the position of the two transects. Transect East is located between 2 km and 10 km to the East of the wind farm and transect West is located between 4 km and 6 km to the West of the wind farm. Along each of the transects, wind speeds are extracted from all available SAR wind maps and averaged over rectangular bins of 1 km (in the transect direction) and 1.5 km (perpendicular to transect direction). Resolution cells showing more than 5 m/s difference from the median within each bin are filtered out as they likely result from reflection from ships.

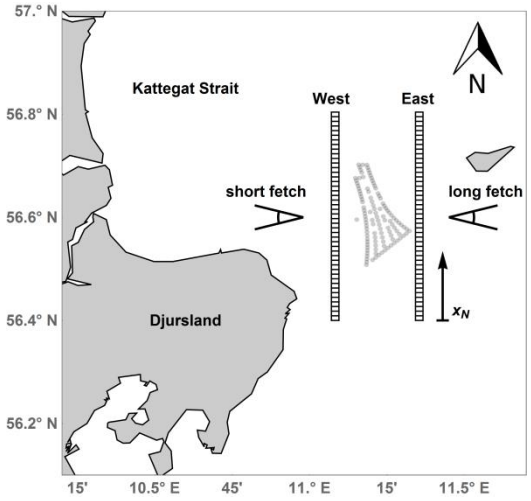

Figure 7: Location of the Anholt wind farm and investigated transects. Two transects "West" and "East" are following the North/South direction.

Wind speed pairs extracted at the same latitude from the East and West transects are assumed to be upstream or downstream of each other for the two directional sectors investigated here. We can calculate the difference Δu_i between upstream and downstream observations depending on x_N:

$$\Delta u_i(x_N) = u_{i,up}(x_N) - u_{i,down}(x_N) \quad (2)$$

where $u_{i,up}(x_N)$ and $u_{i,down}(x_N)$ are the wind speeds on transect "upstream" and "downstream" respectively. From $\Delta u(x_N)$ we can calculate the mean difference $\Delta U(x_N)$ and the standard error $SE(x_N)$. As defined here, a positive ΔU corresponds to a wind speed reduction on the downstream transect.

3.3.1 Long fetch

For situations with Easterly winds the transect "East" is upstream and transect "West" downstream of the wind farm. The fetch is approximately 80 km to the East with exception of the Anholt Island, see Figure 1. A total of 49 SAR wind maps live up to our selection criteria. Of these, 35 were acquired by Envisat before the wind farm was constructed and 14 were acquired by Sentinel-1 after the wind farm construction. Figure 8a shows the average wind speeds along upstream and downstream transects before the wind farm construction. The wind speeds at the same latitude are very similar over the distance 0 km to 32 km. This is as expected since there is open water between the transects and the fetch is long. At 32-37 km where Anholt island is upstream of both transects, the wind speeds on the upstream transect are slightly lower compared to those along the downstream transect. This is likely caused by the lee effects from the island. Figure 8b shows the average wind speed along the two transects after the wind farm was constructed. The wind speed along the downstream transect shows a reduction between 11 km and 30 km. The wind speed along the upstream transect remains between 7.3 and 7.6 m/s from 0 km to 25 km and decreases further North. The number of observations is much lower than before the wind farm construction.

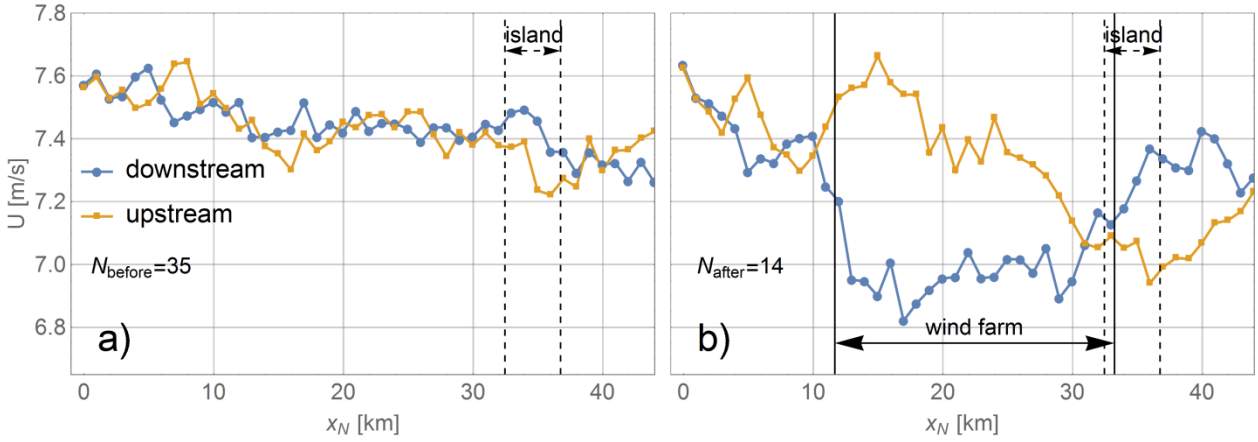

Figure 8: Wind speed transects from a) before and b) after wind farm construction for wind directions between 75° and 105°. East is upstream and West is downstream of the (potential) wind farm location. The position of the wind farm to the East/West and Anholt Island to the East of the transects are indicated.

Figure 9 shows the mean wind speed differences ΔU with one standard error SE indicated by the shaded areas. The average density of turbines between the upstream and downstream transects are shown at the top. Before the wind farm construction, the differences range from -0.2 m/s to 0.2 m/s from 0 km until 30 km. ΔU is negative from 29 km until 37 km around the position of Anholt Island, likely corresponding to a lee effect of the island. After the wind farm construction, the influence of

the wind farm is clearly visible from a difference of 0.3 m/s to 0.75 m/s between 11 km and 27 km. This coincides with the distance where the highest density of turbines is found. Ranges of the standard error shown as the shaded regions are also clearly separated. Around the location of Anholt island, the differences are slightly negative and similar to the differences found before the wind farm construction. At 6 km, a peak around 0.3 m/s appears. The reason for this peak is unclear but could be non-wind effects such as bathymetry-current interaction or remaining effects of hard targets, which influence the radar backscatter and thus the wind speed retrieval.

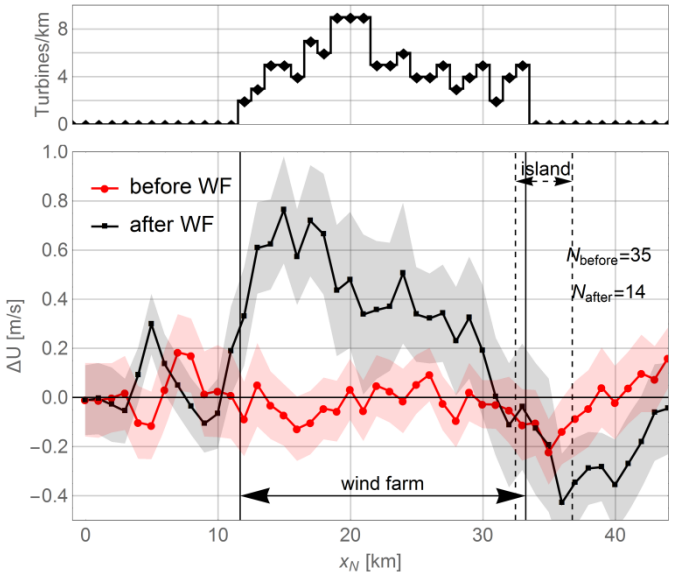

Figure 9: Top: Density of turbines per unit kilometre between the transects. Bottom: Mean difference between wind speeds on the upstream and downstream transect before and after construction of Anholt wind farm. Vertical lines indicate the position of the wind farm and dashed lines the position of the island Anholt to the East. The shaded area represents one standard error around the mean.

A sample size of 35 images creates the baseline of the wind conditions before construction of the wind farm. SAR wind speeds after construction show a clear wake, both absolute and relative to the state before construction of the wind farm, see Figure 8 and Figure 9. Even though the sample size of 14 images after wind farm construction is small, there is clear indication of the wind farm wake.

3.3.2 Short fetch

For situations with westerly winds the transect West is located upstream and transect East is downstream of the wind farm. The fetch is between 16 and 50 km to the West, see Figure 1. Average wind speeds along the two transects are analysed in a similar manner as described for long fetch situations in Sect. 3.3.1. A total of 92 images before and 31 after wind farm construction fulfil the selection criteria. Figure 10 shows the averaged wind speeds. The wind speeds are increasing from South to North along both transects. Wind speeds from before wind farm construction in Figure 10a are consistently lower

for the upstream compared to the downstream transect. This is expected due to the increasing wind speed further offshore. All transects in Figure 10 show lower wind speeds in the Southern end than in the Northern end. This variability in the wind speed is similar to the one found in Sect. 3.2 and likely caused by the variation in fetch along the transects. Wind speed differences and standard error are calculated similar to Sect. 3.3.1 and are shown in Figure 11.

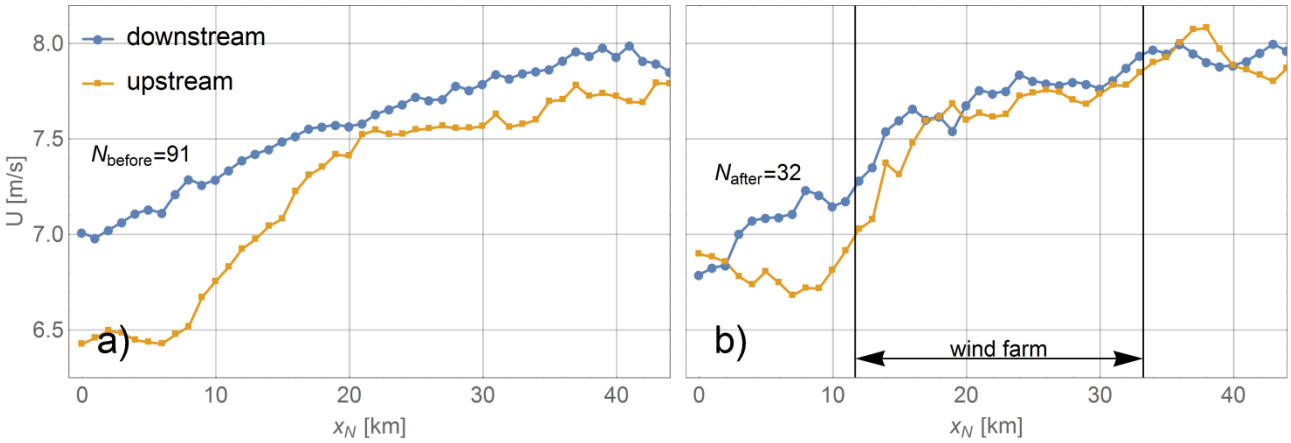

Figure 10: Wind speed transects similar Figure 8 from a) before and b) after construction for wind direction between 255° and 285°. Transect West is upstream and East is downstream of the (potential) wind farm location.

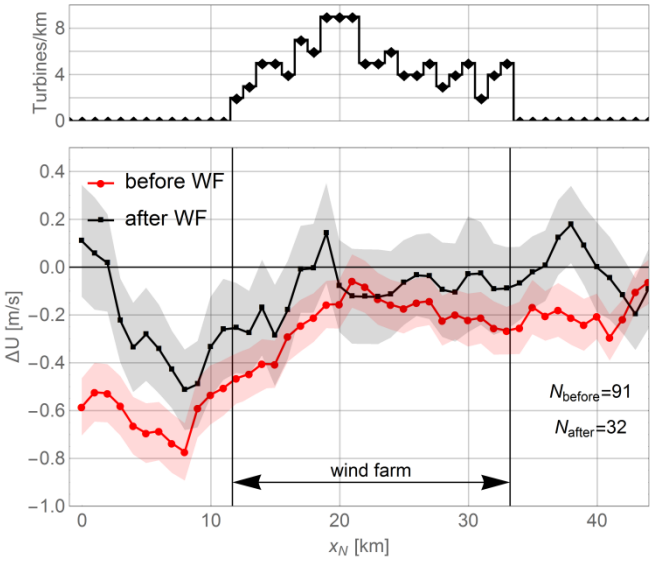

Figure 11: Wind speed difference similar to Figure 9 for short fetch situations with wind directions between 255° and 285°.

The wind speed difference before wind farm construction ranges between -0.7 m/s and -0.4 m/s for the area South of the potential wind farm. Further North from 17 km on the difference ranges between -0.3 m/s and -0.1 m/s. This is consistent

with a short fetch in the South where wind speed is expected to speed up more between the transects than in the Northern part with longer fetches. Wind speed differences after construction of the wind farm show roughly the same pattern except between 0 km and 8 km where differences are large. No clear evidence of wind farm wake effects are found since no significant difference is noted between the average wind speeds before and after wind farm construction. The number of observations before wind farm construction is approximately three times larger than after. The averaged wind speed after construction is less smooth. The convergence to a smoother mean wind speed is expected in the future as more observations from Sentinel-1 A and B become available.

3.4 Wind farm wakes and gradients

To analyse the cumulative effect of coastal wind speed gradients and the wind farm wake effect, four parallel transects are defined perpendicular to the coastline following the orientation of wind turbine row 1. Figure 12 shows a reference transect to the North of the Anholt wind farm (a) and three transects across the wind farm (b, c, and d). Average wind speeds are extracted along these transects similarly to the extraction in Sect. 3.3.

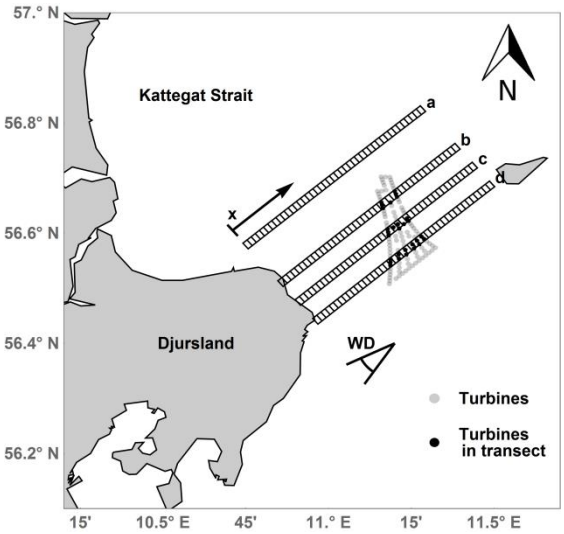

Figure 12: Transects used for analysis of wind farm wakes and coastal gradients. Origin and direction of coordinate x, and the wind direction range (WD) used for the selection of satellite scenes are indicated.

For this analysis, SAR wind maps are selected according to the following three criteria: i) there is full coverage over all four transects, ii) SAR wind speeds at 10 m upstream of the wind farm are between 3 m/s and 12 m/s, and iii) the wind is coming from directions within the sector 214.5°-244.5° centred around the transect orientation and roughly corresponding to the prevailing wind direction at the site. WRF outputs are used to determine the wind direction as described in Sect. 2.4. A total of 57 images before and 35 after the wind farm construction fulfil these criteria.

SCADA wind speeds are extracted for the wind turbine locations covered by transect b, c, and d. The following criteria are used for filtering of the SCADA wind speeds: i) the turbine locations are within the transects and data is available for all those turbines, see Figure 12 ii) SAR wind speeds at 10 m upstream of the wind farm are between 3 m/s and 12 m/s, and iii) the wind is coming from directions within the sector 214.5°-244.5°. A total of 3371 10-minute mean values of SCADA wind speeds live up to these criteria. Data from SAR and SCADA are not collocated in time. The wind turbines are placed in rows oriented from North to South. SCADA wind speeds are averaged for each row segment within each transect.

SAR wind speeds are presented as differences with respect to a reference wind speed, U_{ref} upstream of the wind farm (for transect b, c, and d). For transect a, the reference point is at the same x position as for transect b. SCADA winds are shown as wind speed differences compared to the free stream turbines in row A. Wind speed differences along transects a to d are shown in Fig. 11. Before the wind farm construction, there is a clear coastal wind speed gradient with increasing wind speeds with distance from the coastline for all four transects. For the reference transect a, the deviation between the results before and after wind farm construction is below 0.2 m/s.

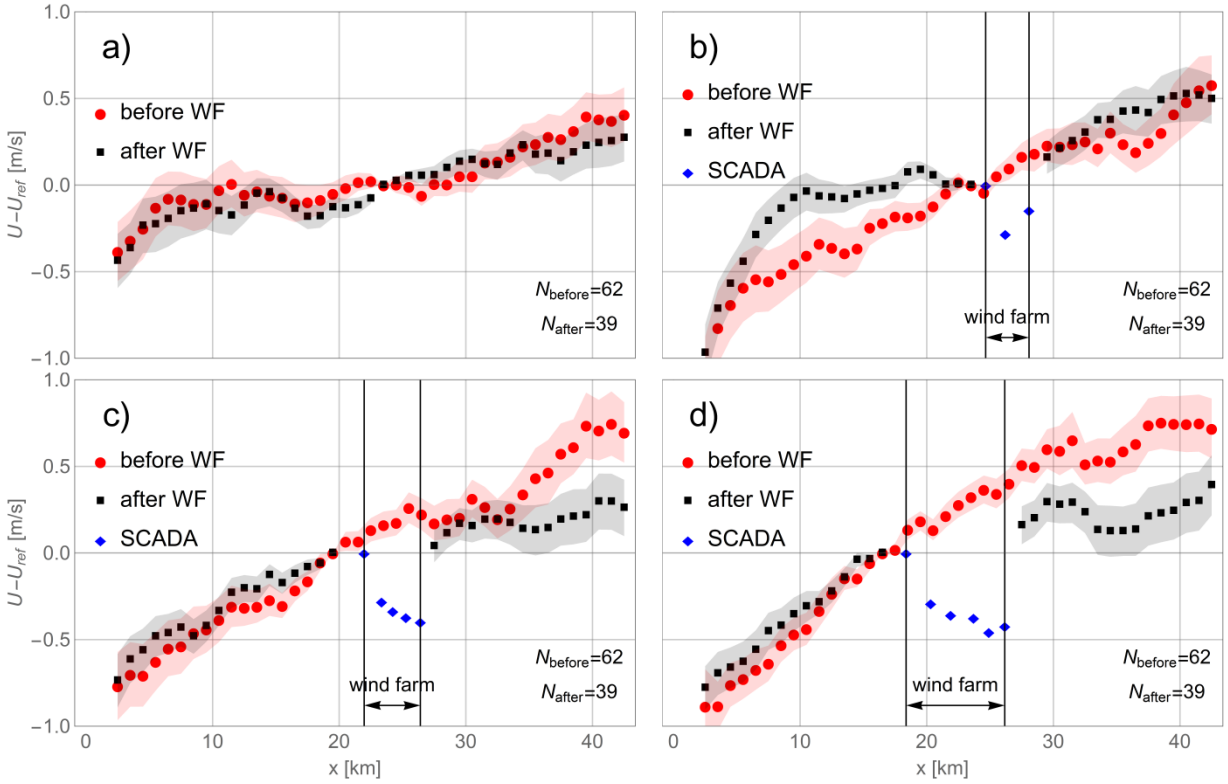

Figure 13: Wind speed differences from SAR along transects a to d before and after construction of the wind farm. Differences calculated from SCADA wind speeds are also shown and the position of the wind farm is indicated.

Upstream of the wind farm, transect b, c, and d clearly show wind speed gradients both before and after wind farm construction. For transect c and d wind speeds differences before and after the wind farm construction agree within 0.2 m/s, whereas larger deviations are found at transect b. These deviations might be caused by variations of the fetch. Wind speed extracts along transect b are likely to be very sensitive to the local wind direction because transect b is located close to the Northern side of the peninsula Djursland. Here, a small change in the wind direction could lead to a large increase or decrease of the fetch, see Figure 12. An increase of the fetch is usually associated with an increase in the wind speed. Therefore, a higher occurrence of wind directions West of 235° after construction of the wind farm could be the reason for the deviations observed for transect b. Transect c and d would be less affected by variations of the wind direction since they are located further South where the fetch varies less for Southwesterly wind directions. The wind direction used for the selection of SAR images comes from WRF simulations at the wind farm location. Any local variability of the wind direction is not resolved by WRF and the true wind direction along the four transects might thus deviate from the WRF wind direction.

Since we do not have in situ measurements for the entire period considered here, it is not possible to determine the exact difference in the wind direction distribution.

Wind speeds downstream of the wind farm show a positive wind speed gradient along transects b, c, and d. Here, the wind speed on transect b is similar before and after wind farm construction. This transect crosses a narrow part of the wind farm with only three turbine rows. Transects c and d cross a larger number of turbines and show a significant change of the wind speed after the wind farm construction and we attribute this change to wake effects of the wind turbines. SAR wind speeds cannot be retrieved correctly within the wind farm itself due to radar reflection from the turbines. The SCADA wind speeds for turbines within transect b to d are used instead to describe the wind speed behaviour within the wind farm. The SCADA wind speeds suggest a reduction of wind speeds downstream of turbine row A which is most pronounced for transect c and d crossing many turbine rows.

SCADA wind speeds show the wind farm wake as a reduction in wind speed compared to the upstream turbine. SAR winds on transect c and d show a reduction of wind speed compared to the situation before construction of the wind farm. The deviations between these two types of wind speed information are between 0.3-0.6 m/s. Differences between SAR and SCADA winds may be attributed to i) a difference in the location with SCADA winds at the turbine positions and SAR winds downstream of the wind farm, ii) differences in the sample size and measurements that are not collocated in time, or iii) differences in the vertical position of the measurements. SCADA data are derived at the turbine operating height whereas the SAR wind retrievals are based on observations of the sea surface. The strongest wind turbine wake effect is expected at the turbine hub height, which is consistent with a stronger wake from SCADA winds compared to SAR.

4 Discussion

We have demonstrated how an extensive archive of SAR wind maps can be used to identify the combined effects of a complex coastal geometry and wind farm wakes on the mean wind conditions around the Anholt wind farm. Our results illustrate how wind maps retrieved from SAR can predict the wind conditions that offshore wind turbines and whole wind farms experience before a wind farm is constructed.

For the first time, wind speeds derived from the SCADA system of an entire wind farm have been compared to SAR wind speeds, see Figure 4. The correlation for free stream conditions is good and the slope of the fit is very close to one. This result is encouraging for using SAR derived mean wind speeds to predict wind conditions as experienced by the wind turbines. GMFs used for SAR wind retrieval are tuned using observational data from buoys in the open ocean. Influences of internal boundary layers caused by the roughness change between land and sea, or effects of limited fetch on the ocean surface roughness are not fully accounted for. These effects are hard to quantify, but the RMSE compared to lidar

measurements in the coastal zone is between 1.3 and 1.4 m/s (Ahsbahs et al. 2017). The SAR wind speed retrieval process needs a wind direction as an input. Readily available SAR wind maps using a global model wind direction are used throughout this study. Therefore, uncertainties in the modelled wind direction translate into errors in the wind speed retrievals.

The Anholt wind farm experiences strong variability in the wind speed along the Western-most row (Row A) for the prevailing wind directions from 245-275°. Comparisons of WRF mean wind variability from the full time series with a downsampled data set matching 72 SAR images before construction show similar results. This strengthens the assumption that the available SAR images correctly represent the mean wind conditions at the Anholt site. The normalized mean wind speed obtained from SAR before construction of the wind farm agrees very well with results from SCADA winds of the first 2.5 years of wind farm operation. The mean wind speed between the South and North of row A increases by 8.7% in the SCADA wind speeds and 8.8% in SAR derived wind speeds, see Table 3. SAR wind maps are thus valuable for characterization of large scale flow phenomena such as wind speed variations over long rows of turbines. Variability in the wind speed relative to a reference location is expected to show little influence from atmospheric stability as presented in Sect. 3.2. The validity of this claim hinges on assumptions of surface layer theory, constant roughness, and stability over the domain. A more detailed study to test these assumptions could support the use of SAR for detection wind speed variabilities.

For this site, nondimensional wind speeds from WRF at the turbine locations also predict wind speed variability very similar to results from SAR and SCADA. Models such as WRF are powerful tools to identify good wind resources, but cannot fully replace observations of the wind conditions on site. The presented analysis of SAR wind maps can complement modelling efforts by introducing an independent measurement for comparison, since both data sets are available before construction of a potential wind farm. A good agreement between WRF and SAR with regard to wind speed variability can add confidence to wind resource assessment. Further studies at locations where the mean wind speed is affected by an upstream shoreline could show if agreement between SAR and NWP modelling is common and if disagreements could point towards an increased uncertainty in the NWP modelled wind resources.

Comparisons in the wake (see Figure 5) showed a lower scatter than free stream comparisons suggesting a better fit in waked compared to free stream conditions, even though the assumptions of a fully developed wind profile are violated by the presence of a wake. Further studies of SAR wind retrievals within wind farm wakes using high quality reference measurements at several heights from the sea surface to the turbine hub height are needed in to examine this finding in more detail.

The correlation of downstream comparison is good but the bias towards higher wind speeds from SAR has increased compared to the analysis upstream of the wind farm, see Figure 4 and Figure 5. The largest wake deficit is located at hub

height (Porté-Agel et al. 2011) and this could cause an overprediction of the SAR wind speed when extrapolated in Figure 5. Additionally, SAR winds are retrieved between 600m and 2600m downstream of the turbine position but are compared to SCADA wind speeds at the turbine location and the wake is likely to recover. This is also consistent with the difference between SAR and SCADA winds in Figure 13. To better quantify wind farm wakes from SAR images, further work is needed to understand how wakes interact with the ocean surface and how this influences SAR wind retrievals.

Anholt wind farm has irregular turbine spacing and the shape is elongated. Methods applied at other offshore wind farm sites for analysing wakes in SAR wind maps (Hasager, Vincent, et al. 2015) are less suitable for Anholt. A new approach for analysing wind farm wakes from SAR images has therefore been suggested here, which explores the difference of SAR wind maps before and after the wind farm was constructed. The wind farm wake effects are analysed along transects approximately perpendicular to the wind direction on the upstream versus the downstream side of the wind farm and along transects crossing the wind farm aligned with the wind direction. For situations with a long fetch, perpendicular transects before wind farm construction provide a suitable baseline to check averaged differences between upstream and downstream transects, see Figure 9. The wind farm wake estimated from SAR shows a structure that roughly follows the turbine density of the wind farm. In contrast, no indication of a wake is found in Figure 11. The wind direction sector overlaps with the sector from Figure 6 where strong horizontal wind speed variability was found, which will also affect the transects. A possible explanation could be that the upstream orography is more complex for the short compared to the long fetch scenario. This could affect the similarity of the wind conditions for the SAR images before and after wind farm construction, either due to difference in the wind direction or atmospheric stratification.

Transects crossing the wind farm can be used to investigate how the coastal wind speed gradient and wakes of the wind farm interact, see Figure 13. No wind speed reductions compared to the upstream reference point are found but two transects going through an area of high wind turbine density show a reduction of the mean wind speed after wind farm construction compared to the situation before. This results stands in contrast to Figure 11 and transect b in Figure 13 where no evidence of a wind farm wake was found. Identification of wakes from SAR images is not trivial when an upstream coastline is influencing the flow. Further studies at locations with simple geometry of the coastline would help to understand the interplay of wind farm wakes and coastal wind speed gradients.

SAR wind maps are suitable for analysing large scale wind conditions and they can show the combined effects of different flow phenomena. In this analysis, wind farm wakes, coastal wind speed gradients, and wind speed variability from differing fetch occur simultaneously. It is challenging to identify the contribution of one particular flow phenomenon, e.g. wind farm wakes from this data. In contrast to engineering wake models such as FUGA or Park that are run with a single wind speed and direction, SAR wind maps capture the full picture of the flow around a wind farm. The presented methods can potentially be repeated for any offshore wind farm site even before the wind farm construction.

The presented SAR data archive goes back to 2002 and offers the possibility of reference measurements before most of the current offshore wind farms were constructed. The analyses presented in this study will gain confidence as the satellite data archives are growing over time. With Sentinel-1 A and B, two new satellites are acquiring new scenes on a daily basis which are available in the public domain. This makes SAR observations and derived wind maps more accessible and the time is right to develop tools for SAR data analysis that are tailored to the needs of the offshore wind industry.

5 Conclusion

Large archives of SAR wind maps have recently become publically available and the sampling frequency of the measurements has increased significantly with the European SAR missions Sentinel-1 A/B. Readily available SAR based wind speed maps represent a computationally and monetarily cheap source of information about the large scale wind speed variability offshore. The maps are available in hindcast and may thus be used from the earliest stages of a wind farm project. We have demonstrated that wind speed maps retrieved from SAR observations of radar backscatter can be used to predict the spatial wind speed variability at a potential wind farm site before construction begins. The satellite based wind speed maps can also be used for characterization of wake effects around existing wind farms and to partially determine the cumulative effects of coastal wind speed gradients and wake effects.

Wind speeds retrieved from SAR correlate well with the SCADA derived wind speeds for the turbines at Anholt wind farm. RMSEs are 2.23 m/s and 2.12 m/s for comparisons upstream and downstream of the wind farm, respectively. Wind farm wakes are detected from SAR wind fields using a long time series with measurements before and after construction of the wind farm. This approach is promising, since a baseline of wind conditions before the construction is available. Wind farm wake effects are found for wind directions leading to a long fetch with a maximum deficit of 0.7m/s. Wind farm wakes at fetch limited conditions are harder to identify possibly due to the complex interplay of different effects such as varying fetch and coastal wind speed gradients on the mean wind speed. More studies using these approaches for different wind farms are necessary, ideally with in situ reference measurements, to determine the capabilities of SAR for wind farm wake detection.

Our results that SAR wind maps can resolve smaller-scale wind variability comparable to SCADA wind speeds. WRF and SAR data sets are independent of each other and are available in the early stages of planning an offshore wind farm. Alongside with model simulations, satellite based wind maps represent a valuable resource to introduce large scale on-site measurements early in an offshore wind farm project, i.e. for planning of on situ measurement campaigns.

Data availability:

SAR wind fields are available at https://satwinds.windenergy.dtu.dk/ and WRF model runs can be made available upon request. SCADA data is not available for publication.

Author contribution:

Tobias Ahsbahs developed methods and code. Merete Badger and Charlotte B. Hasager provided the processed SAR wind maps and contributed with guidance and comments. Kurt S. Hansen prepared the SCADA data and Patrick Volker provided the WRF data. Tobias Ahsbahs prepared the manuscript with contributions from all co-authors. This work is part of Tobias Ahsbahs' PhD under supervision of Merete Badger.

Competing interests:

The authors declare that they have no competing interest.

Acknowledgements:

We would like to acknowledge Ørsted for granting access to data from the Anholt wind farm, Johns Hopkins University Applied Physics Laboratory and the National Atmospheric and Oceanographic Administration (NOAA) for the use of the SAROPS system, and ESA for providing public access to data from Sentinel-1A. Personal thanks to Nicolai G. Nygaard from Ørsted for his approval and comments.

6 References

Ahsbahs, T. et al., 2017. Validation of Sentinel-1A SAR Coastal Wind Speeds Against Scanning LiDAR. *Remote Sensing*, 9(6), p.552.

Alpers, W.R., Ross, D.B. & Rufenach, C.L., 1981. On the detectability of ocean surface waves by real and synthetic aperture radar. *Journal of Geophysical Research*, 86(C7), pp.6481–6498. Available at: http://doi.wiley.com/10.1029/JC086iC07p06481.

Badger, M. et al., 2016. Extrapolating Satellite Winds to Turbine Operating Heights. *Journal of Applied Meteorology and Climatology*, 55(4), pp.975–991.

Barthelmie, R.J. et al., 2007. Offshore Coastal Wind Speed Gradients: issues for the design and development of large offshore windfarms. *Wind Engineering*, 31(6), pp.369–382.

Barthelmie, R.J. et al., 2010. Quantifying the Impact of Wind Turbine Wakes on Power Output at Offshore Wind Farms. *Journal of Atmospheric and Oceanic Technology*, 27(8), pp.1302–1317.

Christiansen, M.B. et al., 2006. Wind resource assessment from C-band SAR. *Remote Sensing of Environment*, 105(1), pp.68–81.

Christiansen, M.B. & Hasager, C.B., 2005. Wake effects of large offshore wind farms identified from satellite SAR. *Remote Sensing of Environment*, 98, pp.251–268.

Dagestad, K.-F. et al., 2013. Wind Retrieval From Synthetic Aperture Radar, an Overview. In *Seasar 2012 Oceanography Workshop*. European Space Agency, ESA.

Dee, D.P. et al., 2011. The ERA-Interim reanalysis: Configuration and performance of the data assimilation system. *Quarterly Journal of the Royal Meteorological Society*, 137(656), pp.553–597.

Dörenkämper, M. et al., 2015. On the Offshore Advection of Boundary-Layer Structures and the Influence on Offshore Wind Conditions. *Boundary-Layer Meteorology*, 155(3), pp.459–482. Available at: http://dx.doi.org/10.1007/s10546-015-0008-x.

Fitch, A.C. et al., 2012. Local and Mesoscale Impacts of Wind Farms as Parameterized in a Mesoscale NWP Model. *Monthly Weather Review*, 140(9), pp.3017–3038. Available at: http://journals.ametsoc.org/doi/abs/10.1175/MWR-D-11-00352.1.

Gade, M. & Alpers, W., 1997. Using ERS-2 SAR images for routine observation of marine pollution in European coastal waters. *Science of the Total Envireonment*, 237–238, pp.441–448.

Gash, J.H.C., 1986. A Note on Estimating the Effect of a Limited Fetch on Micrometeorological Evaporation Measurements. *Boundary-Layer Meteorology*, 35, pp.409–413.

Grachev, A.A. & Fairall, C.W., 1996. Dependence of the Monin-Obukhov Stability Parameter on the Bulk Richardson Number over the Ocean. *Journal of Applied Meteorology*, 36(4), pp.406–414.

Hahmann, A.N. et al., 2015. Wind climate estimation using WRF model output: Method and model sensitivities over the sea. *International Journal of Climatology*, 35(12), pp.3422–3439.

Hansen, K.S. et al., 2015. Simulation of wake effects between two wind farms. *Journal of Physics: Conference Series*, 625.

Hansen, K.S. et al., 2012. The impact of turbulence intensity and atmospheric stability on power deficits due to wind turbine wakes at Horns Rev wind farm. *Wind Energy*, 15(1), pp.183–196.

Hasager, C.B., Mouche, A., et al., 2015. Offshore wind climatology based on synergetic use of Envisat ASAR, ASCAT and QuikSCAT. *Remote Sensing of Environment*, 156, pp.247–263.

Hasager, C.B. et al., 2011. SAR-based wind resource statistics in the Baltic Sea. *Remote Sensing*, 3(1), pp.117–144.

Hasager, C.B., Vincent, P., et al., 2015. Using Satellite SAR to Characterize the Wind Flow around Offshore Wind Farms. *Energies*, 8(6), pp.5413–5439.

Hasager, C.B. et al., 2004. Validation of ERS-2 SAR offshore wind-speed maps in the North Sea. *International Journal of Remote Sensing*, 25(191), pp.3817–3841.

Hersbach, H., 2010. Comparison of C-Band Scatterometer CMOD5.N Equivalent Neutral Winds with ECMWF. *J. Atmos. and Ocean. Technol.*, 27(4), pp.721–736.

Hong, S.-Y., Noh, Y. & Dudhia, J., 2006. A New Vertical Diffusion Package with an Explicit Treatment of Entrainment Processes. *Monthly Weather Review*, 134(9), pp.2318–2341.

Jensen, N.O., 1983. *A note on wind generator interaction (Risø-M-2411)*, Roskilde.

Larsen, G.C., 2009. *A simple stationary semi-analytical wake model*, Risø National Laboratory for Sustainable Energy, Technical University of Denmark.

Li, X. & Lehner, S., 2013. Observation of TerraSAR-X for Studies on Offshore Wind Turbine Wake in Near and Far Fields.

IEEE Journal of Selected Topics in Applied Earth Observations and Remote Sensing, 6(3), pp.1757–1768.

Van Der Laan, M.P. et al., 2017. Challenges in simulating coastal effects on an offshore wind farm. *Journal of Physics: Conference Series*, 854(1).

Monaldo, F.M. et al., 2015. A Weather Eye on Coastal Winds. *Eos*, 96(September), pp.1–8.

Nygaard, N.G., 2014. Wakes in very large wind farms and the effect of neighbouring wind farms. *Journal of Physics: Conference Series*, 524(1), p.12162.

Nygaard, N.G. & Hansen, S.D., 2016. Wake effects between two neighbouring wind farms. *Journal of Physics: Conference Series*, 753(3), p.32020.

Ott, S., Berg, J. & Nielsen, M., 2011. *Linearised CFD Models for Wakes*, Danmarks Tekniske Universitet, Risø Nationallaboratoriet for Bæredygtig Energi.

Peña, A. et al., 2017. On wake modeling, wind-farm gradients and AEP predictions at the Anholt wind farm. *Wind Energy Science Discussions*, 2017, pp.1–18.

Peña, A. & Hahmann, A.N., 2017. *30-year mesoscale model simulations for the "Noise from wind turbines and risk of cardiovascular disease" project*, DTU Wind Energy E, Vol. 0055.

Platis, A. et al., 2018. First in situ evidence of wakes in the far field behind offshore wind farms. *Scientific Reports*, 8(1).

Porté-Agel, F. et al., 2011. Large-eddy simulation of atmospheric boundary layer flow through wind turbines and wind farms. *Journal of Wind Engineering and Industrial Aerodynamics*, 99(4), pp.154–168.

Quilfen, Y. et al., 1998. Observation of tropical cyclones by high-resolution scatterometry. *Journal of Geophysical Research: Ocean*, 103(C4), pp.2156–2202.

Reynolds, R.W., Gentemann, C.L. & Corlett, G.K., 2010. Evaluation of AATSR and TMI satellite SST data. *Journal of Climate*, 23(1), pp.152–165.

Skamarock, W.C. et al., 2008. *A Description of the Advanced Research WRF Version 3*, NCAR Technical Note NCAR/TN-475+STR.

Smedman, A.-S., Bergström, H. & Grisogono, B., 1997. Evolution of stable internal boundary layers over a cold sea. *Journal of Geophysical Research: Oceans*, 102(C1), pp.1091–1099. Available at: http://doi.wiley.com/10.1029/96JC02782.

Stoffelen, A. & Anderson, D., 1997. Scatterometer data interpretation: Estimation and validation of the transfer function CMOD4. *Journal of Geophysical Research*, 102(C3), pp.5767–2780.

Valenzuela, G.R., 1978. Theories for the interaction of electromagnetic and oceanic waves−A review. *Boundary-Layer Meteorology*, 13(1), pp.61–85.

Volker, P.J.H. et al., 2015. The explicit wake parametrisation V1.0: A wind farm parametrisation in the mesoscale model WRF. *Geoscientific Model Development*, 8(11), pp.3715–3731.

Wind Europe, 2018. *Offshore Wind in Europe: Key trends and statistics*, Available at: https://windeurope.org/wp-content/uploads/files/about-wind/statistics/WindEurope-Annual-Offshore-Statistics-2017.pdf.

Wyngaard, J.C., 2010. *Turbulence in the Atmosphere*, Cambridge University Press.